Long-time tails in lattice gases violating detailed balance

R. Brito,* H. J. Bussemaker,† M. H. Ernst, and J. Matsui‡
Institute for Theoretical Physics, University of Utrecht, P.O. Box 80.006, 3508 TA Utrecht, The Netherlands
(Received 21 April 1995)

Using analytic and simulation techniques, we study the long- and intermediate-time behavior of the velocity autocorrelation function in two-dimensional lattice gas automata with stationary states that violate detailed balance. Such models are prototypes of dissipative systems, have stationary states that are very different from Gibbs states, and exhibit long-range spatial correlations. Such static correlations are absent in models with detailed balance symmetry. In some lattice gases with strong violation of detailed balance, the simulations show negative velocity correlations at intermediate times (cage effect), which, to our knowledge, has never been observed in lattice gases before. A mode coupling calculation is used to analyze the long-time tail, whose amplitude is very different from the mean field prediction. When the above static correlations are taken into account, our theoretical predictions agree very well with the results of computer simulations.

PACS number(s): 05.20.Dd, 05.60.+w

I. INTRODUCTION

Equilibrium states of lattice gas automata that violate (semi)detailed balance [1] have curious properties, such as velocity correlations on the same node [2–5] and even long-range spatial correlations [6–8]. These correlations are completely absent in the Gibbs state of lattice gases that satisfy the conditions of (semi)detailed balance.

The observed correlations are closely related to the generic long-range spatial correlations occurring in the stationary states of continuous fluids with externally imposed gradients [9] or in driven diffusive systems [10,6,7]. In the present paper we are only interested in *fluid* models with a locally conserved mass and momentum density.

Very recently dynamical equations for nondetailed balance lattice gas automata have been derived that describe the equilibrium [11,8] and transport [12,13] properties of such lattice gases. The main goal of the present paper is to extend these theories to the computation of current-current time correlation functions in the non-Gibbsian equilibrium state of such lattice gases and to test the theoretical results against computer simulations.

To that purpose we study the long-time behavior of the velocity autocorrelation function $\langle v_x(t)v_x(0)\rangle_{\rm eq}$ of a tagged particle in lattice gases that *violate* detailed balance sufficiently *strongly* so that the equilibrium correlations, affecting the coefficient of the long-time tail, are substantial. For such models, the mean field description of equilibrium properties in terms of completely factorized equilibrium distributions is totally inadequate and one has to use the more refined theory of Ref. [11], which takes dynamic pair correlations into account. The theory of Ref. [12] is not applicable as it is only refers to cases of *weak* violation of detailed balance, where equilibrium correlations can be neglected and only transport coefficients are affected. The equilibrium and transport properties of detailed balance models are well understood at the level of the mean field theory [1], as well as at the more sophisticated level of the ring kinetic theory [14–16].

The existence of long-time tails in the velocity autocorrelation function $\langle v_x(t)v_x(0)\rangle_{\rm eq} \sim A/t^{d/2}$ in discrete d-dimensional fluids is well established through computer simulations and also completely understood and quantitatively explained by mode coupling theories [17–20] and kinetic theories [14,15]. The present paper discusses the existence of long-time tails in lattice gases that violate detailed balance. We restrict our study to three deterministic models that have spatially *uniform* and *stable* equilibrium states, i.e., states that are stable against spatial fluctuations. These restrictions exclude lattice gases with phase separation, such as the models of Refs. [21–25,13], for which a description in terms of Euler and Navier-Stokes equations is not appropriate.

On large spatial and temporal scales the nondetailed balance lattice gases under consideration are described by the Navier-Stokes equations [2,4,3]. It is therefore expected that the long-time tails, which are themselves of hydrodynamic origin, still decay algebraically. However, the coefficient A of the tail will explicitly depend on the size of the static correlations present in the non-Gibbsian equilibrium state.

Let us specify the goals of this paper more precisely. We want to establish theoretically the existence of a long-time tail, derive an analytic expression for the coefficient of the tail in terms of transport coefficients and equilibrium susceptibilities, compute these quantities on the basis of the ring kinetic theory for lattice gases without detailed balance [11], and compare the results with those obtained from computer simulations of long-time tails in the velocity autocorrelation function. An inter-

*Permanent address: Facultad de Ciencias Físicas, Universidad Complutense, 28040 Madrid, Spain.
†Permanent address: IPST, University of Maryland, College Park, MD 20742.
‡Permanent address: Physics Department, Kyushu University, Fukuoka, Japan.

esting new phenomenon, observed in some of our nondetailed balance models, is the occurrence of a cage effect, i.e., negative velocity correlations at intermediate times. The cage effect also occurs in dense classical fluids, but is completely absent in lattice gases satisfying detailed balance.

The paper is organized as follows. In Sec. II we adapt the phenomenological mode coupling theory for lattice gases [17,19] with detailed balance to those without it. Section III is devoted to a description of the microdynamics of tagged and fluid particles together with a brief recapitulation of mean field results and a short description of analytic and numerical results based on the ring kinetic theory of Ref. [11]. The mean field results for the velocity autocorrelation function and the self-diffusion coefficient are derived in the Appendix. Computer simulations of the velocity autocorrelation function, diffusion coefficient, shear viscosity, and susceptibilities are described and analyzed in Sec. IV and compared with theoretical predictions. We conclude with a discussion in Sec. V.

II. MODE COUPLING THEORY

In order to avoid unnecessary technicalities we restrict ourselves to two-dimensional lattice gases defined on a triangular lattice [1] with unit lattice distance, periodic boundary conditions, and $V = L^2$ nodes. At each node, labeled $\mathbf{r}$, there are six *moving* particle states with velocity $\mathbf{c}_i$ $(i = 1, 2, \ldots, 6)$ parallel to nearest-neighbor lattice vectors with $|\mathbf{c}_i| = c = 1$ and a single *rest* particle state $(i = 0)$ with velocity $\mathbf{c}_0 = 0$. Furthermore, evolution occurs at discrete times $t = 0, 1, 2 \ldots$.

The microstate of the system is described by the set of occupation numbers $\{n_i(\mathbf{r}, t)\}$, where $n_i(\mathbf{r}, t)$ equals unity if the state $(\mathbf{r}, \mathbf{c}_i)$ is occupied at time t and vanishes if the state $(\mathbf{r}, \mathbf{c}_i)$ is empty. Double occupancy is excluded (Fermi exclusion rule). The statistical properties of the equilibrium state are described in terms of the average occupation number or single-particle distribution function f_i and the pair correlation function $G_{ij}(\mathbf{r} - \mathbf{r}')$, defined as

$$\begin{aligned} f_i &= \langle n_i(\mathbf{r}) \rangle_{\mathrm{eq}}, \\ G_{ij}(\mathbf{r} - \mathbf{r}') &= \langle \delta n_i(\mathbf{r}) \delta n_j(\mathbf{r}') \rangle_{\mathrm{eq}}, \end{aligned} \tag{1}$$

where the fluctuation is $\delta n_i(\mathbf{r}) = n_i(\mathbf{r}) - f_i$. The dynamics or collision rules have the symmetry of the underlying lattice. Thus, on average, the equilibrium state has the same symmetry. Consequently, $f_i = f_m$ for the moving particle states $(i = 1, 2, \ldots, 6)$ and $f_i = f_0$ for the rest particle state $(i = 0)$. The average node occupation is $\rho = 6 f_m + f_0$.

Due to the Fermi exclusion rule the self-correlation function $(i = j, \mathbf{r} = \mathbf{r}')$ is given by

$$G_{ii}(\mathbf{0}) = f_i(1 - f_i). \tag{2}$$

If the lattice gas satisfies the detailed balance condition, the equilibrium state factorizes over all one-particle states $\{\mathbf{r}, \mathbf{c}_i\}$ and all on- and off-node correlations vanish. The correlation function has the diagonal form

$$G_{ij}(\mathbf{r}) = \delta_{ij} \delta(\mathbf{r}, \mathbf{0}) f_i(1 - f_i). \tag{3}$$

However, in nondetailed balance lattice gas these correlations are nonvanishing [11].

The dynamics of the triangular lattice gases studied here are modifications of the basic seven-bit models of Refs. [1,26], with (semi)detailed balance. In the present paper the detailed balance symmetry is violated by choosing asymmetric forward and backward transition probabilities for collisions that respectively create and destroy a rest particle. The collision rules will be specified in Sec. III. For the tagged particle dynamics we use the collision rules, introduced by Frenkel and collaborators [17,18,27].

To analyze the behavior of a tagged particle we start from the Einstein formula for the coefficient of self-diffusion D, given by $\langle (\Delta x(t))^2 \rangle_{\mathrm{eq}} \simeq 2Dt$ for t large, where the average is taken over an equilibrium ensemble and

$$\Delta x(t) = x(t) - x(0) = \sum_{\tau=0}^{t-1} v_x(\tau) \tag{4}$$

is the x component of the displacement of a tagged particle. With the help of this relation and using the stationarity of the equilibrium state, the Einstein formula for the diffusion coefficient D of a single tagged particle in a discrete space-time system can be transformed into a Green-Kubo-type formula [28], i.e.,

$$D = \sum_{t=1}^{\infty} \langle v_x(t) v_x(0) \rangle_{\mathrm{eq}} + \tfrac{1}{2} \langle v_x^2(0) \rangle_{\mathrm{eq}}. \tag{5}$$

In the context of lattice gases the microscopic velocity of the tagged particle is most conveniently expressed in terms of the occupation number $\overline{n}_i(\mathbf{r}, t)$. This occupation number takes the value unity if the tagged particle is in state $(\mathbf{r}, \mathbf{c}_i)$ at time t and vanishes elsewhere,

$$v_x(t) = \sum_{\mathbf{r},i} c_{ix} \overline{n}_i(\mathbf{r}, t). \tag{6}$$

Consequently, $\sum_{\mathbf{r},i} \overline{n}_i(\mathbf{r}, t) = 1$. Moreover, the equilibrium distribution of the tagged particle is

$$\overline{f}_i \equiv \langle \overline{n}_i(\mathbf{r}) \rangle_{\mathrm{eq}} = f_i / N \tag{7}$$

because the tag is on any of the $N = \sum_{\mathbf{r},i} n_i(\mathbf{r}, t)$ fluid particles with equal probability.

To derive the long-time tail of the velocity autocorrelation function we refer to the mode coupling derivation of Ref. [19] and indicate only where differences occur due to the violation of detailed balance. To start, we write the velocity autocorrelation function in the coarse grained form, where the tagged particle velocity is expressed as a product of tagged particle density times average flow field

$$\langle v_x(t)v_x(0)\rangle_{\rm eq} \equiv \frac{f_m}{N}\sum_{\mathbf{r},i}\sum_{\mathbf{r}_0,j_0} c_{xj_0}c_{xi}\langle \overline{n}_i(\mathbf{r},t)\rangle_s \simeq \frac{f_m}{N}\sum_{r_0,j_0} c_{xj_0}\sum_{r} u_x(\mathbf{r},t)P(\mathbf{r},t). \quad (8)$$

Here the average $\langle\rangle_s$, defined by the first equality, is taken over a special nonequilibrium ensemble, which is conditioned on the tagged particle being in a *moving* state $(\mathbf{r}_0, \mathbf{c}_{j_0})$ at the initial time. The probability for this to happen is $\overline{f}_{j_0} = f_m/N$, which explains the overall factor in front of (8).

In mode coupling theories the time dependence of the probability distribution $P(\mathbf{r},t) = \sum_i \langle \overline{n}_i(\mathbf{r},t)\rangle_s$ of the tagged particle, as well as the local fluid velocity $\mathbf{u}(\mathbf{r},t) = (1/\rho)\sum_i \mathbf{c}_i\langle n_i(\mathbf{r},t)\rangle_s$ in the special initial ensemble, is calculated from the macroscopic equations. This yields, for the Fourier components of tagged particle density and the flow field whose dominant contribution comes from its transverse component,

$$\widehat{P}(\mathbf{q},t) \simeq \exp(-Dq^2t)\,\widehat{P}(\mathbf{q},0),$$
$$\widehat{\mathbf{u}}_\perp(\mathbf{q},t) \simeq \exp(-\nu q^2 t)\,\widehat{\mathbf{u}}_\perp(\mathbf{q},0), \quad (9)$$

where ν is the shear viscosity of the lattice gas.

The only *difference* with the derivation in Ref. [19] is that the initial value of the flow field, calculated in the special initial ensemble $\langle\rangle_s$, contains spatial correlations, i.e.,

$$\mathbf{u}(\mathbf{r},0) = \frac{1}{\rho}\sum_i \mathbf{c}_i\langle \delta n_i(\mathbf{r},0)\rangle_s = \sum_i \mathbf{c}_i G_{ij}(\mathbf{r}-\mathbf{r}_0)/(\rho f_m),$$
$$P(\mathbf{r},0) = \delta(\mathbf{r},\mathbf{r}_0). \quad (10)$$

In fact, this initial condition is identical to the one used in the original derivation of the long-time tail [29] in continuous fluids, where $\mathbf{u}(\mathbf{r},0)$ also contains the equilibrium correlation function. With the help of these results, the velocity autocorrelation function simplifies to

$$\langle v_x(0)v_x(t)\rangle_{\rm eq} \simeq \left(\frac{V}{\rho N}\right)\frac{1}{V}\sum_{\mathbf{q}} e^{-(\nu+D)q^2t} \times \sum_{ij}\hat{q}_{\perp x}(\hat{\mathbf{q}}_\perp\cdot\mathbf{c}_i)c_{jx}\widehat{G}_{ij}(\mathbf{q}) = \frac{1}{2}\frac{\chi_\perp}{\rho^2}\frac{1}{V}\sum_{\mathbf{q}} e^{-(\nu+D)q^2t}. \quad (11)$$

To obtain the second line we have averaged over the equivalent directions x and y and we have introduced the transverse susceptibility

$$\chi_\perp = \lim_{q\to 0}\sum_{i,j}\mathbf{c}_{\perp i}\mathbf{c}_{\perp j}\widehat{G}_{ij}(\mathbf{q}) \equiv \lim_{q\to 0}\langle c_\perp|\widehat{G}(\mathbf{q})|c_\perp\rangle, \quad (12)$$

where $c_\perp = \mathbf{c}\cdot\hat{\mathbf{q}}_\perp$ with $\hat{\mathbf{q}}_\perp$ a unit vector perpendicular to $\hat{\mathbf{q}} = \mathbf{q}/q$. We observe that the second-rank tensor field in (11)

$$\langle \mathbf{c}|\widehat{G}(\mathbf{q})|\mathbf{c}\rangle \equiv \sum_{i,j}\mathbf{c}_i\mathbf{c}_j\widehat{G}_{ij}(\mathbf{q}) = \hat{\mathbf{q}}\hat{\mathbf{q}}\chi_l(\mathbf{q}) + \hat{\mathbf{q}}_\perp\hat{\mathbf{q}}_\perp\chi_\perp(\mathbf{q}) \quad (13)$$

contains in general the longitudinal susceptibility $\chi_l(\mathbf{q})$ and transverse $\chi_\perp(\mathbf{q})$ as two independent scalar fields. If the system is invariant under a discrete group of lattice symmetries, these fields depend on the vector $\mathbf{q}$. If the system would be isotropic, then the susceptibilities would depend only on the magnitude $q = |\mathbf{q}|$. In evaluating the $\mathbf{q}$ sum for a large system, we use the replacement

$$\frac{1}{V}\sum_{\mathbf{q}} \to \frac{v_0}{(2\pi)^2}\int_{\rm 1BZ} d\mathbf{q}, \quad (14)$$

where $v_0 = \frac{1}{2}\sqrt{3}$ is the volume of the unit cell of the triangular lattice. The dominant long-time behavior of (11) is determined by the long-wavelength modes with $|\mathbf{q}| \ll 1$. Therefore we may replace the $\mathbf{q}$ integral over the first Brillouin zone in by an integral over all $\mathbf{q}$ space as in (14). By evaluating the resulting Gaussian integral, the final result for the *long-time behavior* of the velocity autocorrelation function in lattice gases without detailed balance is

$$\langle v_x(0)v_x(t)\rangle_{\rm eq} \simeq \left(\frac{\chi_\perp}{2\rho^2}\right)\frac{v_0}{4\pi(D+\nu)t}, \quad (15)$$

with the initial condition $\langle v_x^2(0)\rangle_{\rm eq} = 3f_m/\rho$. For the normalized velocity autocorrelation function with $\phi(0) = 1$, we have

$$\phi(t) \equiv \frac{\langle v_x(t)v_x(0)\rangle_{\rm eq}}{\langle v_x^2(0)\rangle_{\rm eq}} \simeq \chi_\perp\left(\frac{v_0}{6f_m\rho}\right)\frac{1}{4\pi(D+\nu)t}. \quad (16)$$

In lattice gases *obeying (semi)detailed balance* the occupations of different velocity states at the same or different sites of the lattice are statistically uncorrelated $\langle \delta n_i(\mathbf{r})\delta n_j(\mathbf{r}')\rangle_{\rm eq} = \delta_{ij}\delta(\mathbf{r},\mathbf{r}')f_i(1-f_i)$ and the coefficient in Eq. (16) reduces to $\chi_\perp = 3f(1-f)$, where $f = f_m = f_0 = \rho/7$. The long-time tail for a model with detailed balance becomes then

$$\phi(t) \simeq \left(\frac{1-f}{2\rho}\right)\frac{v_0}{4\pi(D+\nu)t}, \quad (17)$$

with the initial condition $\langle v_x^2(0)\rangle_{\rm eq} = 3/7$. This is the result for lattice gases first obtained by Frenkel and Ernst [17].

The coefficient of the long-time tail in Eq. (16) contains equilibrium quantities such as the density of moving particles f_m and the transverse susceptibility $\chi_\perp$, as well as the transport coefficients of shear viscosity ν and self-diffusion D. To analyze the mode coupling prediction (16) we briefly review in Sec. III the relevant mean field result and quote a theoretical result for the susceptibility, which presents a correction to mean field theory based on ring kinetic theory.

The approach taken in the present paper is to measure the quantities on the right-hand side of Eq. (16) in independent computer simulations, which will be described

in Sec. IV. However, as the measurements of the susceptibilities are very noisy, reaching acceptable statistical accuracy is very time consuming (see Sec. IV). Therefore we also use a theoretical result for the susceptibility in nondetailed balance models, which has been derived in Ref. [8]. Simulations of the susceptibility have only been performed for a few test points.

III. MICROSCOPIC THEORY

A. Collision rules

For a description of the time evolution of lattice gases we refer to [1]. The time evolution of the system consists of strictly local (zero range) collisions, followed by free propagation. The microdynamical equation for the time evolution of the occupation numbers can be written as

$$n_i(\mathbf{r}+\mathbf{c}_i,t+1)-n_i(\mathbf{r},t)=I_i[n(\mathbf{r},t)]. \tag{18}$$

All occupation numbers refer to precollision states. The nonlinear collision term $I_i[n]$ describes p-tuple collisions ($p=2,3,\ldots,6$), defined in terms of a transition probabilities $A_{s\sigma}$ for an input state $s=\{s_i(\mathbf{r},t),\ i=0,1,\ldots,6\}$ to an output state $\sigma=\{\sigma_i(\mathbf{r},t)\}$ at the same node $\mathbf{r}$. Here s and σ represent the set of occupation numbers at node $\mathbf{r}$.

The collisions are specified in terms of the transition matrix $A_{s\sigma}$, with normalization $\sum_\sigma A_{s\sigma}=1$, which only allows collisions that conserve mass and momentum. The probabilities $A_{s\sigma}=\{Q,R,V,W\}$ for collisions with $s\neq\sigma$ in the three nondetailed balance models discussed in this paper are defined in Fig. 1. The colliding configurations are identical to those of the basic seven-bit model of Ref. [26], but the transition probabilities are different. For every input state there are at most two alternative output states with equal probability. By choosing one of the two alternatives at even and one at odd times, the stochastic models can also be implemented as deterministic ones (cf. Ref. [26]). Note that all three models are self-dual, i.e., invariant under exchange of particles and holes.

Lattice gas automata satisfying the semidetailed balance conditions $\sum_s A_{s\sigma}=1$ or the detailed balance conditions $A_{s\sigma}=A_{\sigma s}$ have a Gibbsian equilibrium state without any velocity or spatial correlations [1,5]. In the present models there are at most two different output states for any input state; therefore the semi-detailed balance conditions, combined with the normalization $\sum_\sigma A_{s\sigma}=1$, coincide with the detailed balance conditions. All models discussed in this paper violate the (semi)detailed balance conditions.

B. Mean field theory

We briefly recall the necessary results from mean field theory for nondetailed balance models. The Boltzmann or mean field approximation is obtained by using the Stosszahl ansatz in which p-particle distribution functions are factorized into products of f_i's. Consequently, an average of products $\langle I_i[n]\rangle$ is replaced by a product of averages $I_i[f]$. The resulting equation is the nonlinear lattice Boltzmann equation [2,4,5]

$$f_i(\mathbf{r}+\mathbf{c}_i,t+1)-f_i(\mathbf{r},t)=I_i[f(\mathbf{r},t)]. \tag{19}$$

The nonlinear collision term $I_i[f]$ is a polynomial of degree 7 in the f_i's. The equilibrium solution $f_i(\mathbf{r},\infty)=f_i$ for a spatially uniform equilibrium state is obtained by solving Eq. (19) for its stationary solution

$$I_i[f]=0. \tag{20}$$

Because the equilibrium solution has the spatial symmetry of the underlying lattice, $f_i=f_m$ for moving particles ($i=1,2,\ldots,6$) and f_0 for rest particles. For a given density $\rho=6f_m+f_0$, one has to solve a single polynomial of degree 7 in f_0. This can easily be done numerically, using the iterative method of Ref. [5]. The results are shown in Fig. 2.

The basic distinction between the three types of models is the sign of the slope of $f_0(\rho)$. At low densities, model I has on average a deficit of rest particles because

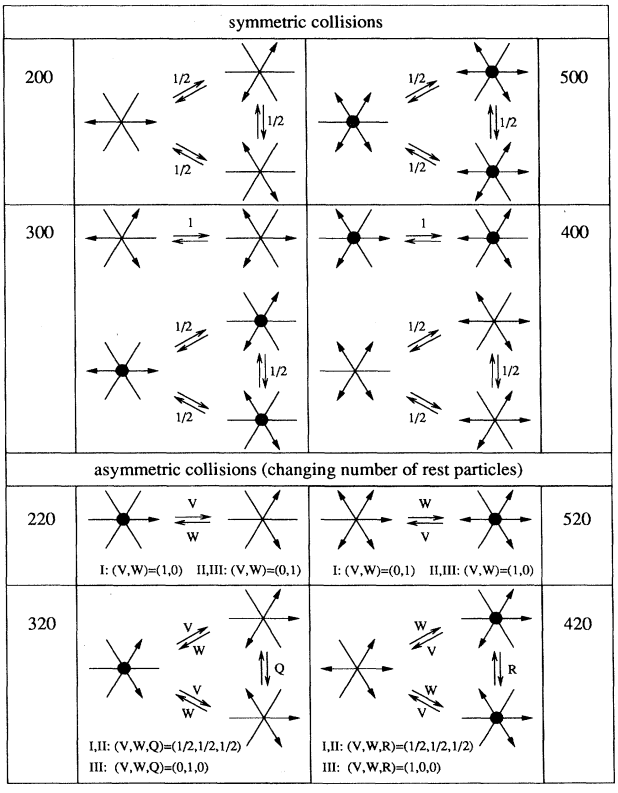

FIG. 1. Collision rules or transition probabilities for the three models used in this paper. Symmetric collisions do not change the number of rest particles and preserve the lattice symmetries. The asymmtric collisions are described by transition probabilities $A_{s\sigma}=\{Q,R,V,W\}$. The triplet of numbers in the left and right columns stands for the number of particles; the x momentum and y momentum of the configuration are as introduced in [26].

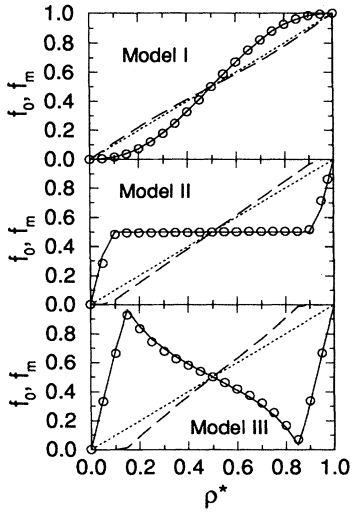

FIG. 2. Average populations of rest (f_0) and moving (f_m) particles versus the reduced density $\rho^* = \rho/7$. The circles represent the results for the average occupations of rest particles obtained in simulations. Solid lines are the mean field predictions for densities of rest particles and dashed lines for moving particles. Finally, dotted lines are the occupation numbers for (semi)detailed balance models $f_0 = f_m = \rho^*$. Note the strong deviations from mean field in models II and III.

the binary collision (220) in Fig. 1 converts rest particles into moving particles. In models II and III the binary collision (220) is reversed and there is an excess of rest particles. This effect is even stronger in model III than in model II because at low densities the collisions (220) and (320) both convert moving particles into immobilized rest particles, which no longer participate in the dynamics. At the lowest densities models II and III do not reach a stationary state. By self-duality, the same applies at the highest densities. Furthermore, in model III the spatially uniform equilibrium state appears to be stable only in the density range $2.35 < \rho^* < 4.65$. For densities outside that interval the sound damping constant is negative and unstable modes drive the system to phase separation [24,30]. The phenomenon of phase separation in lattice gases has recently been reviewed in Ref. [31]. Here we restrict ourselves to stable uniform states. In models I and II the sound damping constant is positive for all densities and uniform states are stable for all values of ρ^*.

To study nonequilibrium properties we linearize the lattice Boltzmann equation (19) around the uniform equilibrium state $f_i(\mathbf{r},t) = f_i + \delta f_i(\mathbf{r},t)$ by making a Taylor expansion of the collision term in (19) and using $I_i[f] = 0$ for the stationary solution, i.e.,

$$I_i(f+\delta f) = \sum_{j=0}^{6} \Omega_{ij}(f)\delta f_j(\mathbf{r},t) + O((\delta f)^2). \qquad (21)$$

This equation defines the linearized Boltzmann collision operator $\Omega_{ij}(f)$, which is a nonsymmetric matrix. Its matrix elements can be evaluated numerically using the equilibrium distribution function f_i, obtained from (20) (see [5]).

Starting from the lattice Boltzmann equation, there exist many different methods to calculate the kinetic pressure, speed of sound, and transport properties for our models, such as the Chapman-Enskog method, or some equivalent multitime scale expansion [1], or by determining the relaxational modes of the linearized lattice Boltzmann equation [32]. Following these standard methods one finds, for the shear viscosity in mean field approximation,

$$\nu = \frac{1}{4}\left(\frac{1}{\omega_\nu} - \frac{1}{2}\right) = \frac{1}{8}\left(\frac{1}{\Omega_{12} - \Omega_{14}} - 1\right), \qquad (22)$$

where $-\omega_\nu$ is an eigenvalue of the linearized Boltzmann collision operator Ω. This eigenvalue has been expressed in terms of matrix elements Ω_{ij}. The numerical value of ν is shown in Fig. 3.

C. Transverse susceptibility

We consider the pair correlation function. In the Boltzmann approximation all correlations $G_{ij}(\mathbf{r})$ between different nodes are neglected, as well as all correlations between different velocity channels on the same node. Only the diagonal part of the correlations as induced by the Fermi exclusion rule is kept in Boltzmann approximation, i.e.,

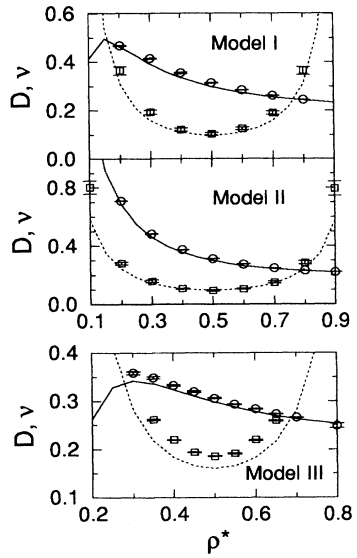

FIG. 3. Transport coefficients (diffusion coefficient D and viscosity ν) versus the reduced density ρ^*. Circles represent the simulated values for the diffusion coefficient, obtained by integration of the velocity autocorrelation function, while the solid line is the mean field prediction for D. Squares are the simulated viscosities measured through the decay of a shear wave. Dotted lines are the mean field values for ν. In model III, with the strongest violation of the semidetailed balance condition, the deviations are the largest.

$$G_{ij}(\mathbf{r}) \simeq G^{(d)}(\mathbf{r}) \equiv \delta_{ij}\delta(\mathbf{r},\mathbf{0})f_i(1-f_i), \tag{23}$$

where f_i is the stationary single-particle distribution function. This result is exact for lattice gases satisfying detailed balance [compare Eq. (3)]. The above result enables us to calculate the susceptibility in mean field approximation as

$$\chi_\perp^0 = \langle c_\perp|\widehat{G}^{(d)}(\mathbf{q})|c_\perp\rangle = 3f_m(1-f_m), \tag{24}$$

where $\widehat{G}_{ij}(\mathbf{q})$ is the Fourier transform of $G_{ij}(\mathbf{r})$ in (23).

In our analysis of the long-time tail (16) we will also use a recent theoretical result, which has been calculated from ring kinetic theory of Ref. [8]. It reads

$$\Delta\chi_\perp = \chi_\perp - \chi_\perp^0 = -\frac{12}{\nu}\left(\nu+\frac{1}{8}\right)^2 \Omega_{13}^{20}(f), \tag{25}$$

where ν is the shear viscosity and $\Omega_{13}^{20}(f)$ is a matrix element of the transition matrix $A_{s\sigma}$, explicitly defined in Ref. [8], that can be evaluated numerically once the stationary solution to the Boltzmann equation (20) is known.

In fact, the matrix elements $\Omega_{ij}^{20}(f)$ represent the amount of on-node (i,j) correlations created in a single collision and vanish in lattice gases without violation of detailed balance. The magnitude of a typical matrix element is a measure for the degree of violation of detailed balance. Table I shows the element Ω_{13}^{20} for the different models I, II, and III at different densities, ordered in increasing degree of detailed balance violation.

IV. SIMULATIONS

A. Transport properties

According to the mode coupling analysis of Sec. II, the long-time behavior of the velocity autocorrelation function contains two static quantities—the density of moving particles f_m and the transverse susceptibility $\chi_\perp$—as well as two transport coefficients—the diffusion coefficient D of the tagged particle and the shear viscosity ν of the lattice gas fluid. These quantities can be obtained from independent computer simulations.

TABLE I. Element $\Omega_{13}^{20}(f)$ for some values of the density ρ^* for the models used in this paper.

Model	ρ^*	Ω_{13}^{20}
I	0.2	+0.002423
	0.3	+0.002366
	0.4	+0.000857
	0.5	+0.000000
II	0.2	−0.003983
	0.3	−0.004164
	0.4	−0.001521
	0.5	+0.000000
III	0.2	+0.001154
	0.3	+0.011521
	0.4	+0.025192
	0.5	+0.031250

The viscosity ν is measured from the decay of macroscopic shear waves; the self-diffusion coefficient D is obtained from (5) by summing the velocity autocorrelation function to the required time. The average occupation numbers $\{f_0, f_m\}$ are obtained by simple counting, after equilibrium has been reached. The susceptibility can in principle be obtained by measuring the small wave number limit of the structure factor, which is the Fourier transform of the pair correlation function $G_{ij}(\mathbf{r})$.

Simulating the macroscopic decay of a shear wave is a nonequilibrium simulation, which requires a different initialization. We use a method described in detail by Gerits *et al.* [25]. We choose a fixed wave vector $\boldsymbol{q} = (0, 2\pi/\lambda)$ with $\lambda = \frac{1}{2}L\sqrt{3}$ in the triangular lattice, which is perpendicular to a lattice vector $\mathbf{c}_1$ (x axis). We need to set up a transverse momentum field $\widehat{g}_\perp(\mathbf{q},0)$, which decays as $\widehat{g}_\perp(\mathbf{q},t) = \widehat{g}_\perp(\mathbf{q},0)\exp(-\nu q^2 t)$. This can be done as follows. For a given density ρ we start from the occupation numbers $\{f_0, f_m\}$ obtained by solving the nonlinear stationary Boltzmann equation (20). The result is shown in Fig. 2. The rest particles are distributed uniformly over all nodes with expected occupation f_0. The moving particle channels $\{\mathbf{c}_1, \mathbf{c}_2, \mathbf{c}_6\}$ are filled with probability $(f_m + a\sin q_y)$ and the channels $\{\mathbf{c}_3, \mathbf{c}_4, \mathbf{c}_5\}$ are filled with probability $(f_m - a\sin q_y)$. Thus the density on the lattice has the constant value $\rho = 6f_m + f_0$, but we have created an initial shear wave $\widehat{g}_\perp(\mathbf{q},0) = 4a\sin q_y$. We have chosen a sufficiently small (here $a = 0.2$) so that no significant nonlinear effects could be observed in the decay.

The above initial state is chosen to get as close as possible to a nonequilibrium state in which the sinusoidal wave can be considered as a small disturbance away from the correlated stationary state. The simulations were carried out on systems of linear dimension $L = 256$ and the exponential decay $\exp(-\nu q^2 t)$ was typically fitted over a time interval from $t = 1000$ to 3000. As mentioned before, we have to wait some time steps (1000 in this case) before performing any measurements, so correlations have been built up. The number of runs was 20 at any given density.

The simulation results for models I and II are shown in Fig. 3. At intermediate densities ($0.35 < \rho^* < 0.65$) the simulated ν in models I and II is very close to its mean field prediction ν in Eq. (22). However, at lower densities the deviation increases to 10% (model I) and 22% (model II) at $\rho^* = 0.3$ and 0.7 and to 17% (model I) and 16% (model II) at $\rho^* = 0.2$ and 0.8. Deviations on the same order of magnitude have been observed [25] in the seven-bit detailed balance model introduced by d'Humières and Lallemand [26] and have been quantitatively explained by ring kinetic theory [16].

However, in model III the behavior is quite different. At the densities studied in the range ($0.35 < \rho^* < 0.65$) of the stable uniform equilibrium states, the measured viscosities are substantially larger than the mean field (MF) prediction; for instance, $\nu = 0.186 \pm 0.008$ (the MF prediction is 0.161) at $\rho^* = 0.5$ and $\nu = 0.219 \pm 0.008$ (the MF prediction is 0.183) at $\rho^* = 0.4$ and 0.6.

One may raise the question whether the viscosity, measured in the macroscopic relaxation experiments, is indeed the linear viscosity, in particular, in model III with its narrow density range of stable equilibrium states where the sound damping constant is small compared to that in models I and II. Consequently, sound wave disturbances decay only slowly and it may be difficult to separate linear and nonlinear effects.

In order to test whether the measured viscosities are strictly linear, we have made an independent measurement of the viscosity by using the following method. We study the average decay of spontaneous fluctuations in the transverse momentum density $\hat{g}_\perp(\mathbf{q},t)$ around the stationary state, described by the hydrodynamic correlation function $F_\perp(\mathbf{q},t) = (1/V)\langle g_\perp(\mathbf{q},t)g_\perp(-\mathbf{q},t)\rangle_{\rm eq}$. In the long-wavelength limit $q \to 0$ this function decays as $F_\perp(\mathbf{q},t) \simeq \chi_\perp(\mathbf{q})\exp(-\nu q^2 t)$.

In general, the statistical accuracy in measuring time correlations in lattice gases at small q is very low [33,34], and therefore the measurements of $F_\perp(\mathbf{q},\mathbf{t})$ are very time consuming. Therefore, we have used this method only in model III, and only at four densities ($\rho^* = 0.35, 0.4, 0.45$, and 0.5) in the stable regime. The results are consistent with the data obtained from shear wave relaxation experiments. The fluctuation measurements take too much time to be of much practical value. The simulation of $F_\perp(\mathbf{q},t)$ for a system of linear dimension $L = 256$ at density $\rho^* = 0.5$ and wave number $q \simeq 0.227$ required for 75 runs takes approximately 90 h of CPU on a DEC-alpha workstation. However, the large deviations between measured and mean field values of transport coefficients are not disturbing. In principle, the "short time" or "bare" transport coefficients entering in the mode coupling derivation of Sec. II contain also corrections coming from correlated ring collisions. Such ring corrections to transport coefficients are only available for lattice gases obeying detailed balance [16] and have not yet been developed for lattice gases with strong violation of detailed balance. The same remarks apply to the smaller deviations between simulations and mean field values for the viscosities [16].

The coefficient of self-diffusion D is obtained from the velocity autocorrelation function, the simulation of which is described below. The transport coefficient D and, by the same token, the viscosity ν are bare (unrenormalized, short-time) transport coefficients [35,36]. We therefore estimate the diffusion coefficient, to be used in (16), by evaluating the sum in (5) over the time interval $t = 0$–$t = 75$.

The simulation results for D are also plotted in Fig. 3 and compared with the mean field theory for self diffusion, as derived in the Appendix. In model I the measured values of D are very close to the mean field prediction. For models II and III the deviations between theory and simulations do not exceed 5% in the relevant density ranges.

B. Static properties

The first problem is how to prepare the stationary state in which the ensemble average (5) is calculated. A spatially uniform (factorized) distribution over all nodes and all velocity channels, specified by the average occupation $f_i = f_0 = f_m = \rho/7$, would be the equilibrium distribution for lattice gases obeying detailed balance. However, the average equilibrium occupations $f_0(\rho)$ and $f_m(\rho)$, observed in simulations, are very different from $\rho/7$, especially in models II and III, and agree very well with the mean field solutions of (20), as is clearly shown in Fig. 2.

However, in the preparation of the initial state we distribute particles with equal probability given by $f_m = f_0 = \rho/7$, with imposed total momentum equal to zero. Then the system is equilibrated during an aging period of $T_{\rm age}$ time steps. The simulations show that the populations reach the equilibrium value in a few time steps at intermediate densities. The system needs the remaining equilibration steps to build up the spatial and velocity correlations observed in equilibrium states of non-detailed balance models [2–5,11]. The aging time chosen depends on the quantities measured, on the model, and on the density.

The mean field results for the average occupations have already been shown in Fig. 2. To compare them with computer simulations, we have considered systems of size L=100 and we have waited an aging period $T_{\rm age}$ of 50, 100, and 500 time steps for models I, II, and III, respectively. The observed occupations were space averaged over all nodes and time averaged over periods of 50–100 time steps and typically 10–20 runs per density point have been performed. The simulations are in excellent agreement with the stationary solutions of the nonlinear Boltzmann equation (20), as already discussed in Ref. [5].

The second equilibrium quantity of interest is the transverse susceptibility $\chi_\perp$ in (13) in the long-wavelength limit. We find from mean field theory $\chi_\perp^0 = 3f_m(1-f_m)$ and from ring kinetic theory $\chi_\perp = \chi_\perp^0 + \Delta\chi_\perp$, with $\Delta\chi_\perp$ given by Eq. (25). In principle, $\chi_\perp(\mathbf{q})$ can be obtained directly from simulations of $F_\perp(\mathbf{q},t)$, described in Sec. IV A, through the initial value $F_\perp(\mathbf{q},0) = \chi_\perp(\mathbf{q})$. The result found in that experiment on model III at density $\rho^* = 0.5$ and $q = 0.227$ is $\chi_\perp(\mathbf{q}) = 0.538$, whereas the prediction (25) from ring kinetic theory yields $\chi_\perp \simeq 0.581$ as $q \to 0$.

The major part of this deviation is not caused by low statistical accuracy of the simulations but by strong dispersion effects in $\chi_\perp(q)$. This can be concluded by evaluating the theoretical prediction for $\chi_\perp(q)$ by the ring kinetic theory of Ref. [11] at wave number $q = 0.227$, yielding $\chi_\perp(q) = 0.547$. As simulations at smaller q values become increasingly time consuming, numerical extrapolation for $q \to 0$ from a sequence of measurements at decreasing q values is not feasible and we use the theoretical result (25) in our analysis of the long-time tails.

C. Velocity autocorrelation at short times

The measurements of the velocity autocorrelation function $\langle v_x(t)v_x(0)\rangle_{\rm eq} \equiv \phi(t)\langle v_x^2(0)\rangle_{\rm eq}$ were performed using the algorithm and programs developed by van der Hoef and Frenkel [18,37]. Their methods are of extremely high statistical accuracy, in particular in the

intermediate- and long-time regimes.

The velocity autocorrelation function appears to be very sensitive to the equal time velocity and spatial correlations existing in the equilibrium state of nondetailed balance models. In order to obtain convergent results it appears necessary to use long equilibration periods. We typically take $T_{\text{age}} = 750$–1000 time steps in all models and even longer in model III at densities close to the stability thresholds $\rho^* = 0.33$ and 0.67, where $T_{\text{age}} = 1500$ was chosen. To discuss the simulation results we distinguish three regimes: short, intermediate, and long-times; we start with short times.

In the Appendix the mean field result $\phi(t) = [\phi(1)]^t = (1-\omega_D)^t$ has been discussed. In detailed balance models this relation is exact for $t = 1$ and 2 [18]. The simplest mechanism to build up dynamical correlations is the recollision, which requires at least two time steps to be completed. Consequently, the resulting correlations can only be observed *after* the second time step, i.e., at $t = 3$, as times are registered just *before* the collisions are taking place.

The same argument applies to dynamic correlations in lattice gases that violate detailed balance. However, the value of $\phi(1)$ is affected by the existing static correlations between the tagged particle and the fluid particles, colliding at a single node. Consequently, the mean field value $\phi(1) = (1-\omega_D)$ is no longer exact. A comparison of the mean field and simulation values of $\phi(1)$ shows that the deviations are small. In model I the deviations are 2% in the intermediate density range $\rho^* = 0.4 - 0.7$ and much smaller ($\sim 0.5\%$) at low and high densities. In model II the corresponding deviations increase from 0.2% at reduced density $\rho^* = 0.1$ to 2.6% at $\rho^* = 0.5$ and to 3.2% at $\rho^* = 0.7$. Finally, in the stable density range of model III the deviations are less than 0.2%. We have also verified that the mean field relation $\Delta = \phi(2) - \phi(1)^2 = 0$, which is exact in detailed balance models, no longer holds and that Δ constitutes a substantial fraction of $\phi(2)$ in all cases studied.

D. Cage effect

Model III, the lattice gas with the strongest violation of detailed balance, shows a cage effect at intermediate times, i.e., the velocity of the tagged particle shows *negative* correlations in the time interval $5 \le t \le 25$, in the whole density range $0.33 \le \rho^* \le 0.67$ of stable uniform equilibrium states. This is shown in Fig. 4, where we have plotted the velocity autocorrelation function ϕ multiplied by t for model III at densities $\rho^* = 0.35$, 0.4, 0.5, 0.6, and 0.65 (from top to bottom). In models I and II the velocity autocorrelation function $\phi(t)$ remains positive at all times. Positivity of $\phi(t)$ is also observed in all lattice gases with detailed balance.

The appearance of a cage effect in the velocity autocorrelation function, which, as far as we know, has never been observed before in lattice gases, is an interesting effect that also occurs in continuous classical fluids at high densities. In high-density configurations a tagged particle is "trapped" in a tight cage formed by surrounding fluid particles, from which it can escape only slowly. However, for the model we are dealing with, the result is the opposite, the cage effect being more pronounced at lower densities rather than at higher ones.

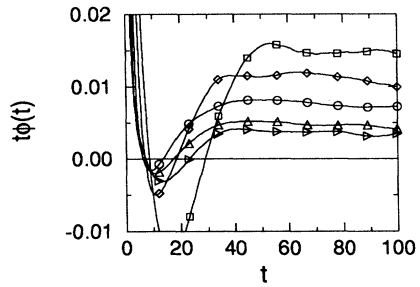

FIG. 4. Cage effect (negative velocity correlations) in the velocity correlation function $t\phi(t)$ in model III at densities $\rho^* = 0.35, 0.4, 0.5, 0.6$, and 0.65, from top to bottom.

The physical processes creating the cage in lattice gases without detailed balance are not yet understood and a quantitative ring kinetic theory for the velocity autocorrelation function is still lacking. For lattice gases obeying detailed balance, Brito *et al.* [15,16] have developed a ring kinetic theory that is in good agreement with the simulated velocity autocorrelation function. It would be interesting to investigate whether ring kinetic theory would be able to account in a qualitative manner, or perhaps even quantitatively, for the cage effect in model III.

E. Long-time tails

The phenomenological mode coupling theory of Sec. II predicts a time dependence of the velocity autocorrelation function as t^{-1}. In order to illustrate this result we have plotted in Fig. 5 the velocity autocorrelation function as a function of time for model I at reduced density $\rho^* = 0.7$. The circles are the simulation results and the solid line is a t^{-1}-decay, plotted as a reference

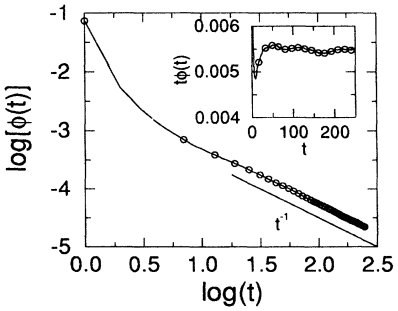

FIG. 5. Natural logarithm of the velocity autocorrelation function for model I at density $\rho^* = 0.7$. The circles are the simulation results and the solid line is a t^{-1} line shown for reference. In the inset the velocity autocorrelation function multiplied by t is plotted versus t. The lattice size is 500×500, the equilibration time 1000, and the number of runs is 250.

line. During the first time steps the velocity autocorrelation function shows an exponential decay, predicted by the mean field theory (see the Appendix). At later times $\phi(t)$ approaches the mode coupling result t^{-1}. The inset of Fig. 5 shows the velocity autocorrelation function multiplied by time t as a function of t, so the asymptotic time regime is transformed into a horizontal line. We see that that regime is reached for times longer than 50.

The amplitude of long-time tail (16) in the velocity autocorrelation function $\phi(t) \sim A/t$ is given by the mode coupling expression

$$A = \left(\frac{\chi_\perp v_0}{6\rho f_m}\right) \frac{1}{4\pi(D+\nu)}. \tag{26}$$

The amplitudes of the long-time tail of $\phi(t)$ measured in computer experiments are shown in Fig. 6. They are compared with the above prediction, where the coefficients are calculated or measured by more and more accurate methods, as follows:

(i) In the simple mean field theory of Sec. III B, which neglects all static correlations, the occupation number of moving particles in Eq. (26) is given by the mean field solution f_m of Eq. (20) (see Fig. 2). The transverse susceptibility is given by $\chi_\perp^0 = 3f_m(1-f_m)$ and the mean field transport coefficients D and ν are shown in Fig. 3. This results into a mean field prediction for A shown as a dotted line in Fig. 6. In models I and II the mean field theory agrees with the simulations within error bars for reduced densities $\rho^* > 0.5$. For smaller densities the simulation results are systematically outside the error bars and smaller than the mean field predictions. In model III mean field theory disagrees with the simulations at all densities.

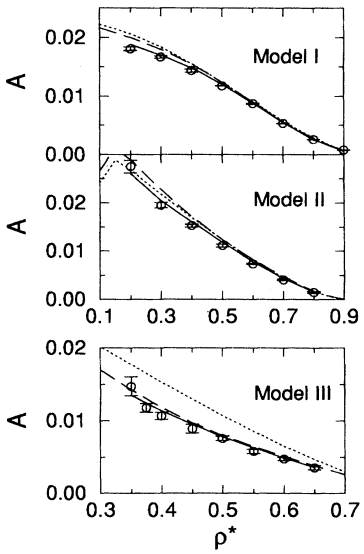

FIG. 6. Amplitudes of the long-time tail of the velocity autocorrelation function. Circles are the simulation results with the corresponding error bars, obtained by fitting $t\phi(t)$ to a constant at long-times. The lines represent the mode coupling expression Eq. (26) evaluated in different approximations: dotted lines are obtained from mean field $\chi_\perp$, D, and ν values; dashed lines are from mean field D and ν values and ring kinetic $\chi_\perp$ values; solid lines are from simulated ν and D values and ring kinetic $\chi_\perp$ values.

(ii) At the next level of refinement we use the susceptibility $\chi_\perp = \chi_\perp^0 + \Delta\chi_\perp$ predicted by ring kinetic theory with $\Delta\chi_\perp$ defined in Eq. (25). However, we still use mean field values for f_m, ν, and D. This prediction for the amplitude is represented by a dotted line in Fig. 6. The effect of the $\Delta\chi_\perp$ correction is small in models I and II, i.e., a slight decrease of the predicted amplitude of 2.2% at $\rho^* = 0.3$ and 0.7% at $\rho^* = 0.4$ in model I and a slight increase of 4.3% at $\rho^* = 0.3$ and 1.3% at $\rho^* = 0.4$ in model II. It leads to slightly better (model I) or slightly worse (model II) agreement between theory and simulations. However, in model III the corrections $\Delta\chi_\perp$ from ring kinetic theory are substantial (see Fig. 6) and lead to a decrease of the amplitude of 19%, 22%, and 25% at reduces densities $\rho^* = 0.35$, 0.4, and 0.5, respectively. This constitutes a great improvement for the agreement between theory and simulations.

(iii) As already mentioned in Sec. IV A, the mean field predictions for the transport coefficients are rather poor (10–20 %) at low and high densities in models I and II and increase to 23% in model III. In our final comparison of simulated long-time tails with the amplitude from mode coupling theory, we replace the transport coefficients in Eqs. (16) and (25) by their simulated values, described in Sec. IV A. Simulated transport coefficients are in most cases larger than the mean filed values, so the amplitude of the long-time tail decreases and makes the agreement with the simulated velocity autocorrelation function better. The resulting predictions for the amplitudes are shown by the solid line in Fig. 6. There is good agreement between theory and simulations of the long-time tail of the velocity autocorrelation function in lattice gas with weak or strong violation of the detailed balance conditions.

V. CONCLUSION

The main goal of this paper on long-time tails is to perform and analyze a consistent set of *computer simulations*, in which not only the long-time tail of the velocity autocorrelation function has been measured but in which also all phenomenological coefficients, entering in the mode coupling expressions for these tails, are obtained from independent computer experiments. These quantities are the shear viscosity, measured from the decay of macroscopic decay of shear waves, and the self-diffusion coefficient, obtained by integrating the velocity autocorrelation function. Moreover, we have measured by simple counting the equilibrium occupations of moving and rest particle states, as well as the equilibrium susceptibilities, which are the Fourier transforms of the pair correlation functions. On the *theoretical* side we have extended the mode coupling theory of [19,18] to non-detailed balance models. The result for the amplitude of the long-time tail differs in two key static quantities—the average occupation of moving particles f_m and the

transverse susceptibility $\chi_\perp$—from the corresponding results for detailed balance models. Furthermore, we have calculated all transport coefficients, susceptibilities, and average occupations from the available mean field and ring kinetic theories.

The ring kinetic theory of [11,8] gives excellent agreement with the computer simulations for all three models studied and for all density ranges of interest. If one would use instead the mean field values for the static and transport coefficients entering in the amplitude of the long-time tail, the predicted long-time tail would be strongly at variance with the simulation results.

The velocity autocorrelation function in one of the nondetailed balance models studied here shows the so-called *cage effect*, i.e., negative velocity correlations, an effect very familiar in the theory of dense classical fluids. This is, to our knowledge, the first time that such cage effects have been observed in lattice gases with only zero range interactions.

The relatively large deviations between mean field predictions and simulated values of the transport coefficients in Fig. 3, in particular in model III, as well as the observed cage effect remain unexplained. It would be very interesting to investigate whether the existing deviations can be explained by extending the ring kinetic theory of Ref. [11,8,13] to transport coefficients in nondetailed balance models.

ACKNOWLEDGMENTS

The authors are very grateful to D. Frenkel and M. van der Hoef, who have made their computer codes for simulating the velocity autocorrelation function in lattice gas automata available to us, without which this investigation would not have been possible. R.B. acknowledges support by DGICYT (Spain) under Contract No. PB91-0378 and a grant of the Ministerio de Educación (Spain). H.J.B. is financially supported by the "Stichting voor Fundamenteel Onderzoek der Materie," which is sponsored by the "Nederlandse Organisatie voor Wetenschappelijk Onderzoek." M.H.E. acknowledges financial support from the Offices of International Relations from Complutense and Utrecht University for a visit to Complutense University. J.M. acknowledges support from Kanazawa University, which enabled him to spend a year at Utrecht University.

APPENDIX: TAGGED PARTICLE PROPERTIES

The dynamics of a single tagged particle in a fluid of untagged particles is described in Refs. [17,18]. Mean field theory for the velocity autocorrelation function and the coefficient of self-diffusion in detailed balance models has been developed in Ref. [27]. Here we only indicate the modifications with respect to Ref. [27] resulting from the violation of detailed balance. The velocity autocorrelation function $\phi(t)$, defined in (16), is in mean field theory given by

$$\phi(t) = (\phi(1))^t \equiv (1-\omega_D)^t. \tag{A1}$$

Consequently, the diffusion coefficient follows from (5) as

$$\begin{aligned} D &= \langle v_x^2(0)\rangle_{\rm eq}\left(\sum_{t=0}^{\infty}\phi(t) - \frac{1}{2}\right) \\ &= \langle v_x^2(0)\rangle_{\rm eq}\left(\frac{1}{\omega_D} - \frac{1}{2}\right). \end{aligned} \tag{A2}$$

The tagged particle dynamics is described by the so-called maximally random collision rules [27]. To calculate $\phi(1)$ we need the *expected* velocity $\overline{\mathbf{v}}(1|\mathbf{c}_0) \equiv (1-\omega)\mathbf{c}_0$ of a tagged particle with initial velocity $\mathbf{c}_0$ after one time step. In an encounter of p *particles* at node $\mathbf{r}$ with input configuration $s(\mathbf{r}) = \{s_i(\mathbf{r}),\ i = 0,1,2,\ldots 6\}$ and $p = \rho(s) = \sum_i s_i(\mathbf{r})$, the tag is with equal probability on any of the p occupied output states $\sigma_i(\mathbf{r})$ and the expected postcollision velocity of the tagged particle is $(1/p)\sum \mathbf{c}_i\sigma_i(\mathbf{r}) = \mathbf{g}(\sigma)/\rho(\sigma) = (1/p)\sum_i \mathbf{c}_i s_i(\mathbf{r})$. In mean field approximation the probability to have a precollision configuration $s(\mathbf{r})$, given that the tag is on the incoming velocity $\mathbf{c}_{j0}$, reads

$$\bar{F}_0(s) = \prod_{j\neq j_0}^{6} f_j^{s_j}(1-f_j)^{1-s_j}, \tag{A3}$$

where f_i is the stationary solution of Eq. (20). The expected velocity $\overline{\mathbf{v}}(1|\mathbf{c}_{j0})$, summed over all p-tuple collisions, i.e., over all configurations $s(\mathbf{r})$ with the incoming tag in channel $\mathbf{c}_{j0}$, is then

$$\overline{\mathbf{v}}(1|\mathbf{c}_{j0}) = \sum_s \left(\frac{\mathbf{g}(s)}{\rho(s)}\right)\bar{s}_{j0}\bar{F}_0(s)\mathbf{c}_{j_0} \equiv (1-\omega)\mathbf{c}_{j0}. \tag{A4}$$

This quantity can be calculated following [27] with the result

$$\begin{aligned} \phi(1) = 1-\omega_D = (1-f_0)(1-f_m)^5\Bigg\{1 + 2x + 2x^2 + x^3 \\ + \frac{1}{5}x^4 + x_0\left[\frac{1}{2} + \frac{4}{3}x + \frac{3}{2}x^2 + \frac{4}{5}x^3 + \frac{1}{6}x^4\right]\Bigg\}, \end{aligned} \tag{A5}$$

where x and x_0 are defined as

$$x = f_m/(1-f_m), \quad x_0 = f_0/(1-f_0). \tag{A6}$$

[1] U. Frisch, D. d'Humières, B. Hasslacher, P. Lallemand, Y. Pomeau, and J. P. Rivet, Complex Syst. **1**, 649 (1987).
[2] B. Dubrulle, U. Frisch, M. Hénon, and J. P. Rivet, J. Stat. Phys. **59**, 1187 (1990).
[3] J. A. Somers and P. C. Rem, in *Numerical Methods for the Simulation of Multi-Phase and Complex Flow*, edited by T. M. M. Verheggen, Lecture Notes in Physics, Vol. 398 (Springer-Verlag, Berlin, 1992), p. 59; D. van Coevorden, M. H. Ernst, R. Brito, and J. A. Somers, J. Stat. Phys. **74**, 1085 (1994).
[4] M. Hénon, J. Stat. Phys. **68**, 353 (1992).
[5] H. J. Bussemaker and M. H. Ernst, J. Stat. Phys. **68**, 431 (1992).
[6] B. Schmittmann and R. K. P. Zia, in *Phase Transitions and Critical Phenomena*, edited by C. Domb and J. L. Lebowitz (Academic, London, 1995).
[7] P. L. Garrido, J. L. Lebowitz, C. Maes, and H. Spohn, Phys. Rev. A **42**, 1954 (1990).
[8] M. H. Ernst and H. J. Bussemaker, J. Stat. Phys. (to be published).
[9] J. R. Dorfman, T. R. Kirkpatrick, and J. Sengers, Annu. Rev. Phys. Chem. **45**, 213 (1994).
[10] G. Grinstein, D. H. Lee, and S. Sachdev, Phys. Rev. Lett. **64**, 1927 (1990).
[11] H. J. Bussemaker, M. H. Ernst, and J. W. Dufty, J. Stat. Phys. **78** 1521 (1995).
[12] B. Boghosian and W. Taylor (unpublished).
[13] H. J. Bussemaker, Ph.D. thesis, University of Utrecht, 1995, and unpublished.
[14] T. R. Kirkpatrick and M. H. Ernst, Phys. Rev. A **44**, 8051 (1991).
[15] R. Brito, and M. H. Ernst, Phys. Rev. A **44**, 8384 (1991).
[16] G. A. van Velzen, R. Brito, and M. H. Ernst, J. Stat. Phys. **70**, 811 (1993); R. Brito and G. A. van Velzen, J. Stat. Phys. (to be published).
[17] D. Frenkel and M. H. Ernst, Phys. Rev. Lett. **63**, 2165 (1989).
[18] M. A. van der Hoef and D. Frenkel, Phys. Rev. A **41**, 4277 (1990); M. A. van der Hoef and D. Frenkel, Physica D **47**, 191 (1991).
[19] M. H. Ernst, Physica D **47**, 198 (1991).
[20] T. Naitoh, M. H. Ernst, and J. W. Dufty, Phys. Rev. A **42**, 7187 (1990).
[21] D. Rothman and J. M. Keller, J. Stat. Phys. **52**, 1119 (1988).
[22] C. Appert and S. Zaleski, Phys. Rev. Lett. **64**, 1 (1990).
[23] F. J. Alexander, I. Edrei, P. L. Garrido, and J. L. Lebowitz, J. Stat. Phys. **68**, 497 (1992).
[24] H. J. Bussemaker and M. H. Ernst, Physica A **194**, 258 (1993).
[25] M. Gerits, M. H. Ernst, and D. Frenkel, Phys. Rev. A **48** 988 (1993).
[26] D. d'Humières and P. Lallemand, Complex Syst. **1**, 599 (1987).
[27] M. H. Ernst and T. Naitoh, J. Phys. A **24**, 2555 (1991).
[28] M. H. Ernst, *Liquids, Freezing and the Glass Transition*, 1989 Les Houches Lectures, Session LI, edited by D. Levesque, J. P. Hansen, and J. Zinn-Justin (Elsevier, Amsterdam, 1991), p. 43.
[29] M. H. Ernst, E. Hauge, and J. M. J. van Leeuwen, Phys. Rev. A **4**, 2055 (1971).
[30] H. J. Bussemaker and M. H. Ernst, Transp. Theory Stat. Phys. **23**, 147 (1993).
[31] D. H. Rothman and S. Zaleski, Rev. Mod. Phys. **66**, 1417 (1994).
[32] S. P. Das, H. J. Bussemaker, and M. H. Ernst, Phys. Rev. E **48**, 245 (1993).
[33] A. Noullez and J. P. Boon, Physica D **47**, 212 (1991).
[34] P. G. Grosfils, J. P. Boon, R. Brito, and M. H. Ernst, Phys. Rev. E **48**, 2655 (1993).
[35] M. A. van der Hoef and D. Frenkel, Phys. Rev. Lett. **66**, 1591 (1991).
[36] J. A. Leegwater and G. Szamel, Phys. Rev. Lett. **67**, 408 (1991).
[37] M. van der Hoef, Ph.D. thesis, University of Utrecht, 1992 (unpublished).